5.4 Reactive transport modeling

V. Montoya, F. Huber, D. Leone, N. Ait Mouheb, M. Trumm, T. Schäfer, V. Metz

Introduction

Advanced numerical methods are needed to quantitatively assess and predict radionuclide migration and geochemical evolution of different systems of interest for nuclear waste disposal by reactive transport modelling approaches. Quantitative calculations of radionuclide release and migration are necessary to evaluate the safety functions of the different engineered barriers and geometry included in a geological disposal concept.

The understanding of the evolution of a deep repository system over geological time scales requires a detailed knowledge of a series of highly complex coupled processes. By using small-scale laboratory experiments, under well-defined boundary conditions, numerical modelling can provide information to help in the repository design and predict future radionuclide migration in case of an incident in the post-closure phase

Research activities on reactive transport modelling during 2016 have been focused on coupled advective or diffusive transport processes with different chemical reactions (sorption, precipitation, aqueous speciation, kinetics). As a site for high level waste (HLW) disposal has not yet been selected in Germany, research in the reactive transport field deal with all relevant host rock types (rock salt, clay and crystalline rock) in close cooperation and interaction with strong national and international academic partners as well as waste management organizations.

At this moment, there are different systems under study in a laboratory scale where reactive transport modelling is applied:

- Diffusion and sorption of radionuclides in illite and montmorillonite.
- Diffusion in the interface low pH cement / clay system (EU Horizon2020 CEBAMA project) and study of the change in the pore structure.
- Diffusion and precipitation in sea sand and clay.
- Migration of redox sensitive radionuclides in fractured crystalline rock.

Other system where transport processes are modelled also includes:

- Modelling the effect of fracture geometry on the bentonite erosion.
- Simulation of colloid transport in artificial and real gap geometries.

This kind of calculations in the laboratory scale can provide the scientific basis for the performance assessment of various repository design options. Additionally, reactive transport modelling tools have also been used to predict radionuclides release / retention under various geochemical boundary conditions in the near-field of a generic repository scenarios in an argillaceous host rock (ENTRIA project).

The reactive transport simulations described previously, have been conducted with different codes depending on the studied system: PHREEQC v. 3 [1] and COMSOL Multiphysics ® 5.0 [2]. Additionally, the interface iCP [3] has been used and tested taking advantage that KIT-INE is part of the Consortium where this tool has been developed. One of the advantages of using these codes is that all of them are in continuous development. This interface provides a numerical platform that can efficiently simulate a wide number of multiphysics problems coupled to geochemistry (i.e. liquid flow, solute and heat transport, elastic and plastic mechanical deformations and geochemical reactions).

Modelling of coupled processes at the low pH cement / clay interface

This work is included in a PhD in the framework of the EU Horizon2020 CEBAMA project and includes experimental and modelling studies of interface processes between a low pH cement (50% CEM I 52.5N + 50 silica fume) and a MX-80 bentonite pore water and assess the specific impact on HTO, $^{36}Cl^-$, $^{129}I^-$ and Be migration. The modelling work supports the interpretation of the experimental results and help to identify possible missing parameters and enhance the process understanding.

The reactive transport model consists of a one dimensional (1D) fully water saturated isothermal (298 K) problem representing a laboratory through diffusion experiment of HTO, Be(II) $^{36}Cl^-$, and $^{129}I^-$ across the interface bentonite pore water/low pH cement. Geometrical and initial transport parameters including the discretization of the system have been implemented (see Figure 1). The mesh size and the time steps have been selected to ensure a satisfactory compromise between computation time and sufficient spatial resolution of the expected geochemical and transport processes, especially at the interface between the bentonite pore water and the low pH cement hydrated phases. A constant and no-flux bound-
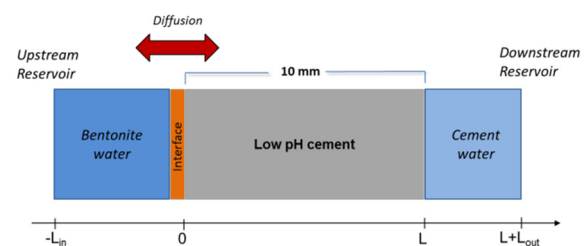

Fig. 1: *Schematic representation of the diffusion experiments*

ary condition has been imposed on the extremities of the upstream and downstream reservoir, respectively.

Considering the very low permeability of cement mass transport will be considered diffusion driven only, following Fick's law.

$$J = -D \frac{\partial C}{\partial x}$$

where J is the substance flux [kg/m^2·s]; $\partial C/\partial x$ is the concentration gradient [kg/m^4]; and D is the diffusion coefficient [m^2/s]. In the absence of data concerning the effective diffusion in low pH cements, a value of 10^{-10} m^2/s was selected. The effective diffusion coefficient was then related to the porosity evolution according to the Archie's law. Initial porosity of the cement has been determined experimentally by mercury intrusion porosimetry (MIP). Additionally, porosity changes due to mineral precipitation/dissolution and feedback on the effective diffusion coefficient are also taken into account in the model considering the molar volumes of the different solids formed or dissolved. Electrostatic surface interactions are not included, although they may influence the transport of the anionic tracers $^{36}Cl^-$, $^{129}I^-$ and $Be(OH)_3^-$ [4].

The system studied is implemented in the code PHREEQC v.3 [1] which can take into account geochemical and physical parameter variations due to mineralogical evolution as a function of time. The initial mineralogical composition of the cement hydrated phases considered is representative of a low pH cement (pH ~ 11.0) with 93 wt-% being form by C-S-H phases with a Ca:Si ratio of 0.8. Mineralogical composition has been determined experimentally with a combination of different techniques (X-ray diffraction (XRD), thermogravimetric - differential thermal analysis (TG-DTA), ^{29}Si and ^{27}Al Magic angle spinning nuclear magnetic resonance (^{29}Si and ^{27}Al MAS NMR) and scanning electron Microscopy - energy dispersive X-ray spectroscopy (SEM-EDX) At this moment, it has not been possible to experimentally identify the solid phase containing iron and for this reason we have assumed that iron phases are in the form of Fe-ettringite. The initial pore water composition of the low pH cement is defined in equilibrium with the hydrated solid phases present in the system and in agreement with the measured concentrations. The pore water composition of the clay is representative of the MX-80 bentonite described in the literature [5] and has been synthetized and measured in the laboratory.

Chemical reactions at equilibrium and kinetically controlled have been simulated using the thermodynamic database Cemdata07 available in PHREEQC format [6]. Debye-Hückel equation, valid for the ionic strength of the studied system (< 0.3 M) is preferred to save computational time. Cemdata07 includes hydrates commonly encountered in Portland cement systems in the temperature range 0 - 100°C. Rate equations of precipitation/dissolution of secondary / primary phases are provided directly in the input files

of PHREEQC. Kinetic parameters for C-S-H phases and ettringite have been selected from [7, 8].

In the present status, sorption of the tracers in the cement matrix is not included in the model, sorption reactions of $^{36}Cl^-$ and $^{129}I^-$ and Be into the low pH cement matrix will be considered by a thermodynamic mechanistic sorption model to be implemented in PHREEQC. The recent review of Ochs et al. (2016), [9] will be considered to select the most appropriate sorption parameters, as well as the data generated in this PhD work with batch experiments.

The simulations were carried out for different contact times (14 min, 5 and 30 days) predicting that the low pH cement will be damaged in contact with the bentonite pore water, having a degraded area of ~2 mm after one month of alteration. The alteration on the low pH cement is mainly due to the partial dissolution of C-S-H phases resulting in an increase of the porosity. The carbonation is linked to the precipitation of calcite and thus the decalcification of C-S-H phases. Magnesium enrichment in the decalcification area has been reported in the literature [10, 11]. In our system, brucite is undersaturated and attempts to model the magnesium perturbation using available thermodynamic data suggested the formation of hydrotalcite. However, the recent determination of the solubility data for M-S-H phases will make it possible to account for the potential formation of M-S-H phases [11] and will be considered in the future. Finally, no attempts have been done to model the iron evolution and the diffusion of HTO in the system will reach the steady state after 5 days of interaction.

Modelling the effect of fracture geometry on bentonite erosion

The effect of fracture geometry on bentonite erosion has been studied by means of numerical simulations. The 2D model for the sodium bentonite erosion used in this work was developed and applied by Neretnieks, Liu and Moreno [12,13,14]. For a thorough discussion on the governing equations describing the bentonite expansion and erosion the reader is referred to the literature given above. The model is applicable for simplified chemical system where bentonite is represented by a sodium montmorillonite and only monovalent cations (1-100 mM) are present in the groundwater. Figure 2 gives an overview of the model geometry and boundary conditions for the flow and mass transport. The model is implemented in the finite element code COMSOL Multiphysics V5.2 [2].
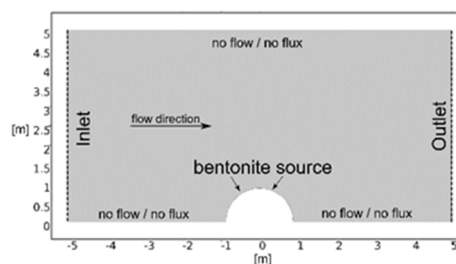

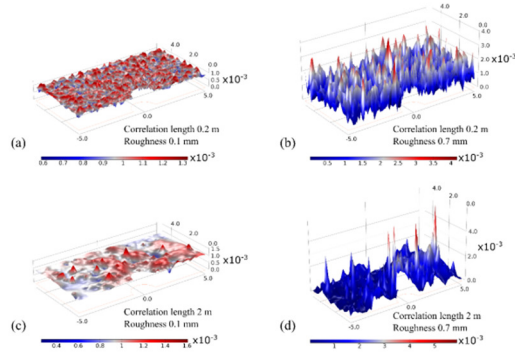***Fig. 2:*** *Model geometry and boundary conditions*

Fig. 3: Aperture fields for a correlation length of 0.2 m for STD of 0.1 mm (a) and 0.7 mm (b) and a correlation length of 2 m for STD of 0.1 mm (c) and 0.7 mm (d). Please note that a superelevation factor of 1200 was used.

A triangular mesh with 13362 elements is used for the numerical simulation.

So far, the model considered only a parallel plate fracture with a constant aperture (1 mm). To examine the effect of heterogeneous fracture geometry random normal aperture distributions with correlation lengths of both 0.2 m and 2 m and a mean aperture of 1 mm have been generated for different standard deviations (STD; equivalent to surface roughness of 0.1 mm, 0.3 mm, 0.5 mm and 0.7 mm). Based on these aperture distributions hydraulic conductivity fields were calculated with the Cubic Law [15] and subsequently used in the Darcy equation to calculate the fracture flow fields. A two-way coupling between the flow and the bentonite erosion process is considered.

A range of mean fracture flow velocities was covered in the study (1×10^{-5} m/s, 1×10^{-6} m/s and 1×10^{-7} m/s, respectively). Generally speaking, the heterogeneous aperture fields induce flow channeling and
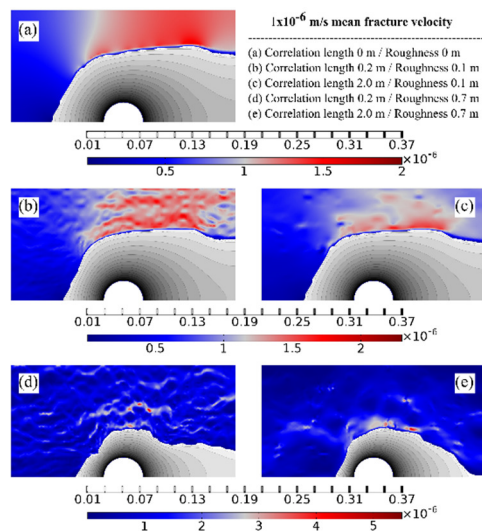

Fig. 4: Bentonite erosion patterns (greyish areas) and flow fields (red-blue colorbar) for STDs of (a) 0 mm, (b) 0.1 mm CL 0.2 m, (c) 0.1 mm CL 2 m, (d) 0.7 mm CL 0.2 m, (e) 0.7 mm CL 2 m for 1×10^5 m/s.
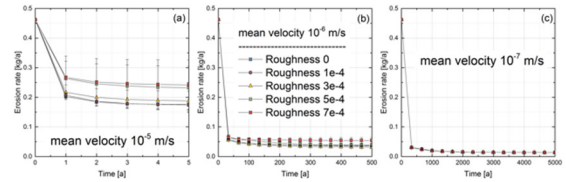

Fig. 5: Calculated erosion rates for the CL of 2 m

therefore locally varying shear forces which lead to irregular bentonite expansion and erosion patterns. Figure 4 shows results for the bentonite erosion for a mean fracture flow velocity of 1×10^{-6} m/s. The extent of swelling into the fracture decreases for increasing roughness due to higher flow velocities/shear forces.

Figure 5 shows simulated erosion rates [kg/a] for the 2-m correlation length aperture fields. With respect to the two different aperture correlation lengths used, no dependency on the erosion rate results was found. In case of the highest mean flow velocity (1×10^{-5} m/s), a clear trend is visible. That is, the erosion rates correlate significantly with increasing roughness ($\geq 3\times10^{-4}$ m). The highest mean erosion rates (~0.24 kg/a) are ~40% higher than the erosion rate for the homogeneous case (~0.17 kg/a). Even extreme values of ~0.33 kg/a were calculated yielding an increase of up to ~95 %. For decreasing mean flow velocities, the impact of fracture geometry on the erosion rates starts to decrease. Only 33% increase in erosion rates are found for the 1×10^{-6} m/s case.

For 1×10^{-7} m/s mean velocity no impact of roughness was found (0.013 kg/a; increase of < 1% only). Here, the variability in shear forces due to the heterogeneous flow field are not high enough to lead to an increase in erosion rate. The results obtained verify the importance of fracture heterogeneity on the bentonite erosion for mean velocities higher than ~1×10^{-7} m/s.

References
[1] Nardi A., et al. (2014) *Computers & Geosciences,* **69,** 10-21.
[2] COMSOL (2014) COMSOL-Multiphysics. Version 5.0, www.comsol.com
[3] Parkhurst and Appelo (2013) C. A. J. U.S. Geological Survey Techniques and Methods, 2013, book 6, chap. A43, 497 p.
[4] Chagneau, A., et al. (2015). *Env. Sci. & Tech. Letters*, **2**, 139–143.
[5] Wersin, P. (2003). *Journal of Contaminant Hydrology,* **61,** 405-422.
[6] Lothenbach, B. and Winnefeld, F (2006) *Cement and Concrete Research* **36**–2, 209–226.
[7] Marty, N. et al (2015). *Applied Geochemistry*, **55**, 108-118.
[8] Baur, I., et al. (2004). *Cement and Concrete Research,* **34**, 341–348
[9] Ochs, et al. (2016). Springer International Publishing Switzerland.
[10] Jenni, A. et al. (2014) *Phys. Chem. Earth A/B/C* **70–71**, 71–83.
[11] Dauzeres, A. et al. (2016) *Cem. Concr. Res.*, **79** 137–150

[12] Neretnieks, I., et al. (2009) SKB Technical report TR-09-35. Svensk Kärnbränslehantering AB, Stockholm, Sweden.

[13] Moreno, L., et al. (2011) *Physics and Chemistry of the Earth, Parts A/B/C* **36**, 1600-1606.

[14] Liu, L., et al. (2009) *Langmuir* **25**, 679-687.

[15] Witherspoon, P.A., et al. (1980). *Water Resources Research* **16**, 1016-1024.